Electronic Supplementary Material (ESI) for Nanoscale.

Polymer-Metal Coating for high contrast SEM cross sections at the deep nanoscale

Daniel Staaks[1,2], Deirdre L. Olynick[1], Ivo W. Rangelow[2] and M. Virginia P. Altoe[1],

[1] Molecular Foundry, Lawrence Berkeley National Laboratory, Berkeley, 94720, United States
[2] Ilmenau Univ. of Technology, Dept. of Micro- and Nanoelectronic Systems, 98684, Germany

SUPPORTING INFORMATION

Sup. A Polymer damage and spin speed curve 2
Sup. B Effect of lower acceleration voltage 3
Sup. C Contrast in the scope of this work 4
Sup. D Contrast perception dependence on the signal-to-noise ratio 5
Sup. E Visibility improvement by contrast 6
Sup. F Monte Carlo Simulation of BSE and FSE 7
Sup. G Coating variations - PMMA 8
Sup. H Coating variations – Carbon 9
Sup. I Residual free removal of CPM coating 10
Literature 11

Sup. A Polymer damage and spin speed curve

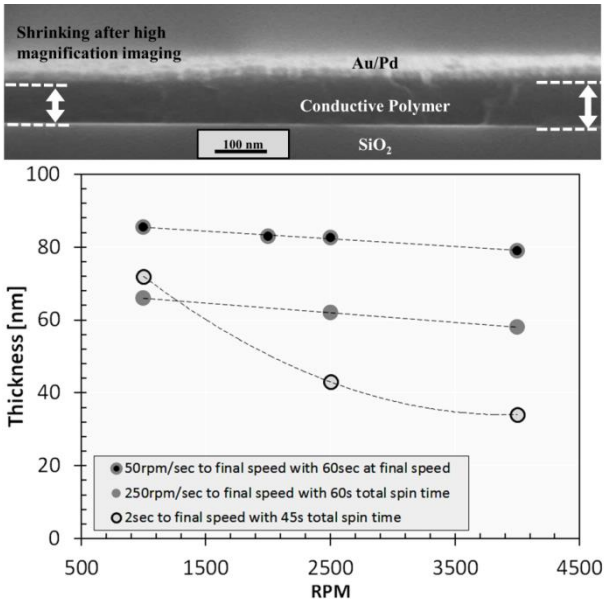

Figure A: Top: CS SE image of CPM coating after (left) and before (right) high magnification electron beam exposure of cross-section. Coating shrinks by about 20%. **Bottom:** Spin speed curves for Aquasave polymer at different angular acceleration and spin time, using shrunk thickness values.

The coating recipe used acceleration of 50 rpm/s and spin time was 50 s at 2500 rpm final speed. The process was tested down to 5 mm x 5 mm sample size. Slow acceleration was preferred, as the risk of sample loss due to centrifugal forces is strongly reduced.

Note that the bake temperature of 150°C for Aquasave differs from manufacturer recommended temperature (100°C) for use as top coat film on electron beam resist. Also, thermal stability of polyaniline compounds has been shown to greatly exceed 180°C[1,2]. Furthermore, polyaniline as an aromatic compound offers higher stability against beam damage[1].

The final thickness of the conductive polymer can be adjusted by spin speed. Because Aquasave tends to shrink by about 20% of its original value upon high magnification (>50k) electron beam irradiation, thickness measurements of the polymer were done after shrinking. Commonly known spin speed behavior of thickness $\propto 1/\sqrt{\omega}$ (ω is angular velocity) was obtained for high acceleration (≥ 500 rpm/s), whereas slower acceleration (≤ 250 rpm/s) resulted in linear behavior.

Sup. B Effect of lower acceleration voltage

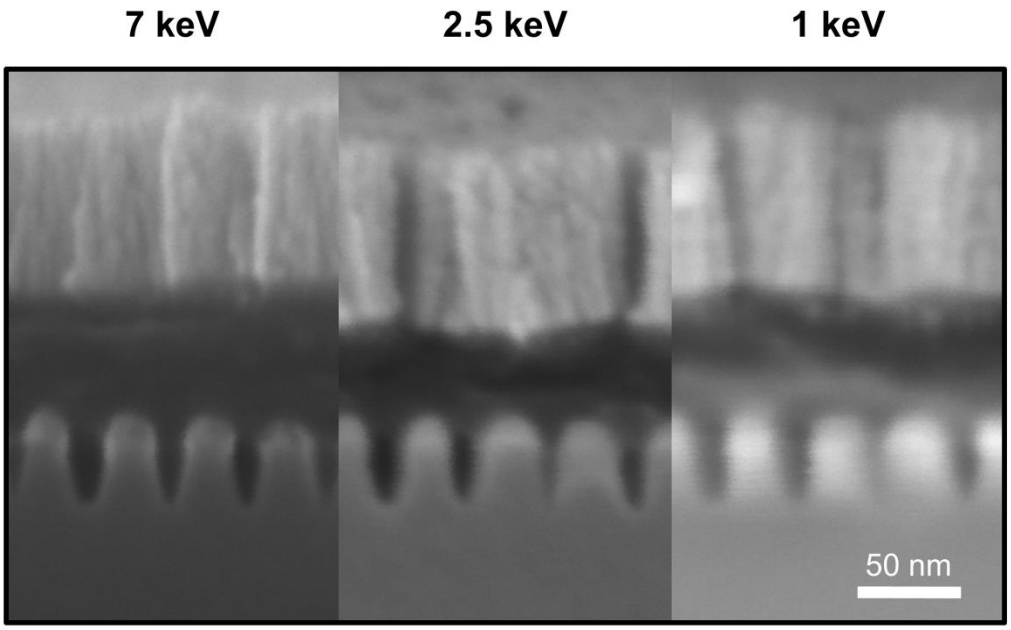

Figure B: SE image of Sample type 3 (see Sup D) with CPM coating (70 nm Au/Pd). Different acceleration voltages are compared: 7 keV, 2.5 keV and 1 keV.

Figure B shows CPM coating with different acceleration voltages of 7 keV, 2.5 keV and 1 keV. Note that the resolution decreases significantly for these 15 nm trenches with decreasing voltage. Also note that decreasing the voltage increases the secondary electron yield, which causes materials to appear brighter.
At lower beam voltage the same contrast effect is visible. The difference is that reducing the acceleration voltage increases the secondary electron yield and thus increases the overall brightness. Resolution loss, however is a critical issue for single-digit feature imaging and therefore not ideal at these dimensions.

SUP. C CONTRAST IN THE SCOPE OF THIS WORK

In an SEM, local contrast differences can be affected by every variation of the signal along its processing path in the hard and software between the electron emission from the specimen and the display of the image. Before the image is saved to a file, its information content can be altered with respect to the previous signal processing. For example, the SEM contrast control, changes the gain to the photo multiplier which increases the intensity range of the image, whereas the SEM brightness control changes the voltage offset of the photomultiplier.
This means, that upon detection, the hardware processing, amplification and internally processing by the imaging software must be kept the same within the same experiment in order to maintain the same conditions.
Between different experiments however, the SEM contrast and brightness controls have to be adjusted depending on imaging conditions and sample to obtain images without gray level cutoff in the high key (high gray level intensities) or low key regions of the corresponding histogram.

Sup. D Contrast perception dependence on the signal-to-noise ratio

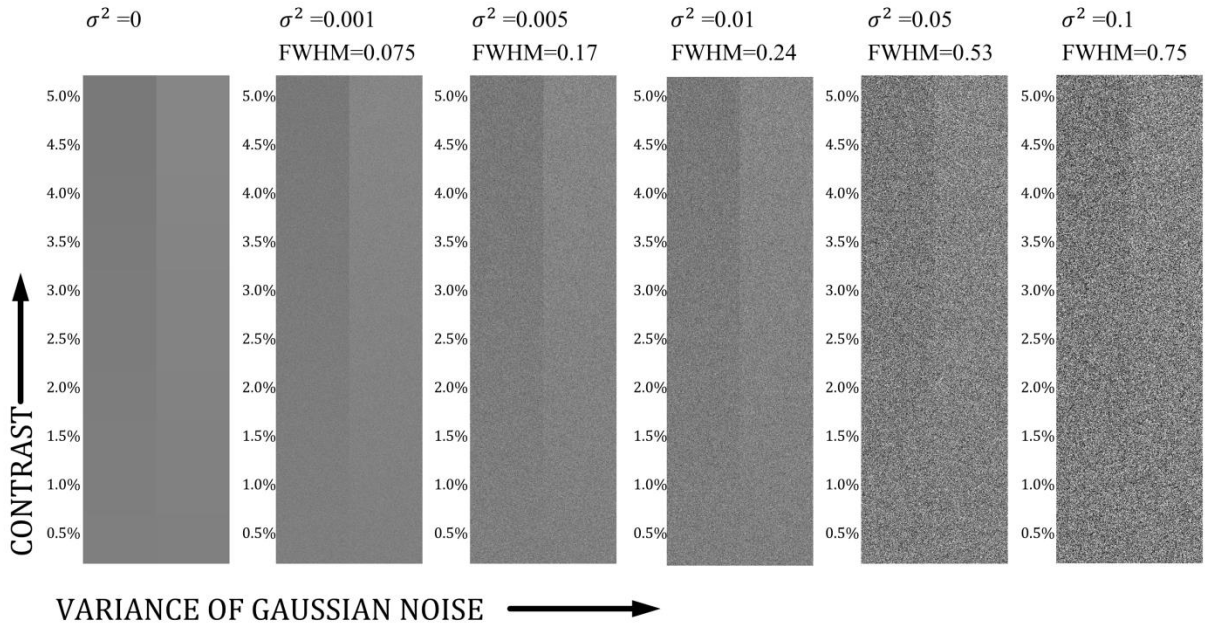

Figure D: Plot comparing contrast as a function of variance of Gaussian noise between $\sigma^2 = 0$ and $\sigma^2 = 0.1$. Every field compares the same 10 levels of contrast ranging from 0.5% to 5%. Every contrast level has two subfields with gray levels that are symmetrically spread to the center gray level 128 (8 bit image) and are calculated between the mean values of the two distributions. Each subfield gray level was superimposed with Gaussian noise and subfields were then stacked together. This shows that visibility is not only a function of contrast, but also of Gaussian noise variance.

White Noise can be characterized as the variance σ^2 of a Gaussian distribution and affects contrast perception shows *Figure **D*** six fields, of which each consists of 20 subfields, where each two horizontally adjacent subfields a normalized contrast $C_N=C_S/S_{max}$ of 0.5% and 5% . Introducing Gaussian noise by increasing the variance leads to a decrease in visibility of the interface, despite having the same contrast in all 6 fields. At $\sigma^2 = 0.1$ the contrast differences at the lowest contrast levels can not be discerned, demonstrating that interface resolution depends on contrast and noise levels in each imaged area. Because contrast distributions can be asymmetric/non-Gaussian in real images, we use the full width at half max (FWHM), instead of variance, as a measure of noise. Broadening the distribution by a factor of 10 in FWHM leads visibly to a decrease in resolution in *Figure **D*** how far features of certain contrast can be distinguished by the human eye is a physiological question of sensitivity and spatial frequency[3–5] and is not being discussed here. An estimate would be the Rose criterion $\Delta S > 5S_{Noise}$, which states that the signal difference needs to be at least 5 times the noise level to be distinguishable by eye[6,7].

Sup. E Visibility improvement by contrast

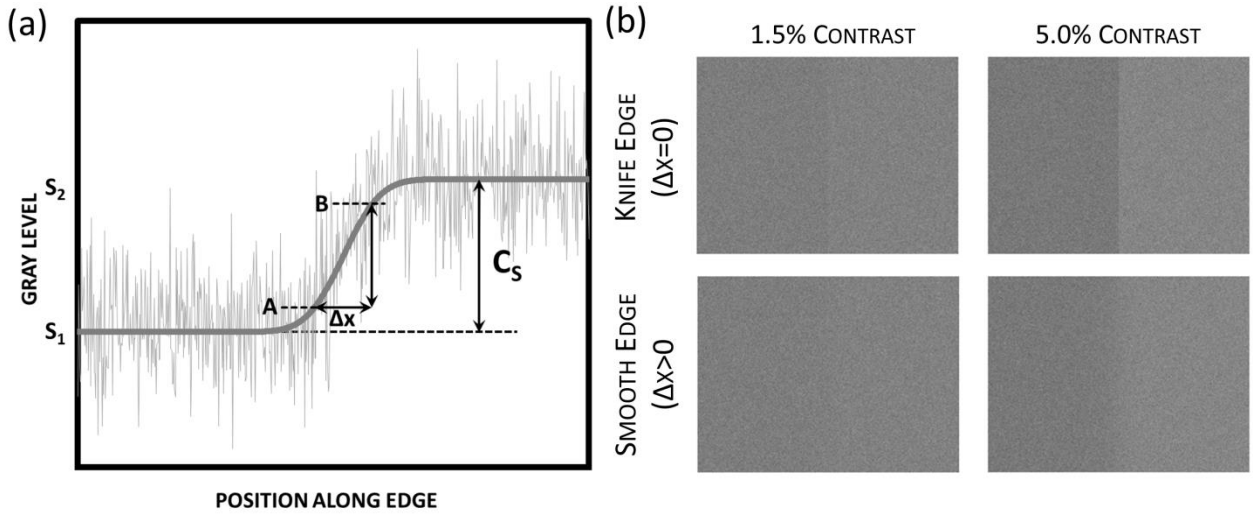

Figure E: (a) Schematic of gray level over position along an feature edge, corresponding to Figure 2. A and B denote 1sigma difference (16% and 84%) for determining resolution as a measure of electron probe size Δx. Signal contrast is C_S. **(b)** Visibility change with contrast. A exemplary knife edge (Δx=0) with ultimate resolution and a smooth edge Δx>0 are compared. Note that the knife edge is visible for both contrast differences, while at the smooth edge a contrast enhancement makes the feature visible.

High contrast and high resolution are both required when imaging features at the single-digit nanoscale. Resolution however, can be seen either quantitatively or qualitatively, and is usually defined by the minimum spacing at which two separate points can be recognized as distinct and separate. At the technical limits of imaging in SEM it is therefore important to clarify the visibility connection to contrast and the signal-to-noise ratio.

Figure (a) shows the schematic of the signal along an edge corresponding to Figure 2. The resolution can be seen as Δx in a smooth edge with Δx>0. Infinite resolution (Δx=0) and real edges with smooth transition (Δx>0) are compared in *Figure (b).* Real edges usually have smoother transitions and therefore have additional blur. *Figure (b)* simulates knife edges and smooth edges at two levels of $C_N=C_S/S_{max}$ contrast, 1.5% and 5% (according to *Figure* in *Sup.* ***D*** with $\sigma = 0.001$). In each case an edge scan from left to right was done and plotted with its gray level as function of position. To reduce the noise, 10 line scans were averaged to obtain the edge scan. This would compare to a 10 nm long edge with 1 nm pixel size. Even at the low level of contrast, the knife edge is clearly visible. On the other hand, the smooth transition with the same contrast can barely be distinguished by eye. Typically real samples have smooth instead of knife edge transition. This means that the contrast has to be higher to resolve the feature.

Sup. F Monte Carlo Simulation of BSE and FSE

Simulation was done using CASINO 3d simulation software ver. 3.3.0.4.

Apart from BSE simulation, the software also allows for secondary electron simulation, but as the authors state themselves[8], secondary electron emission is very sensitive to the used physical model. The software uses plasmon theory to generate secondary electrons[9] and was tested for metal[9] and silicon[8]. However, we are not certain whether the software models SE emission correctly for polymers, where SE generation can be complex[10].

For all simulations, physical models were chosen to be:
Total cross section: Mott by Equation (Browning [1994]) (Monsel)
Partial Cross Section: Mott by Equation (Browning [1994]) (Monsel)
Radom Number Generator: Lagged Fibonacci (Boost lf607)
Directing cosin: Lowney [1994] (Monsel)
dE/dS Calculation: Joy and Luo + Lowney (Monsel)
Ionisation Potential: Joy and Luo [1989] (Monsel)
Incident Electron Options: Minimum electron energy[No Sec. generation]: 0.05

Layer Preset:

	SIZE			**PHYSICAL PROPERTY**
Material	**X [nm]**	**Y[nm]**	**Z[nm]**	**Density [g/cm³]**
Silicon	2000	2000	2000	2.33
Polyaniline	50	2000	2000	1.4
Au/Pd	Varied	2000	2000	15.52

For side views of cross-sections in Figure 6 (a-d):
Microscope Properties:
Number of simulated electrons: 1000
Energy: 7 keV
Beam diameter: 1 nm

For plots in Figure 6 (e-f):
Microscope Properties:
Number of simulated electrons: 10000
Energy: 7 keV
Beam diameter: 1 nm
Spacing: 0.4 nm
Data points across line: 500
Tilt angle: -0.7deg across y axis

Sup. G Coating variations - PMMA

Sample type 3: Patterned SiO_2 with Cr mask (30 nm pitch). Fabrication was done like Sample 2, but Cr mask was left on and pattern is not etched as deep as Type 2.

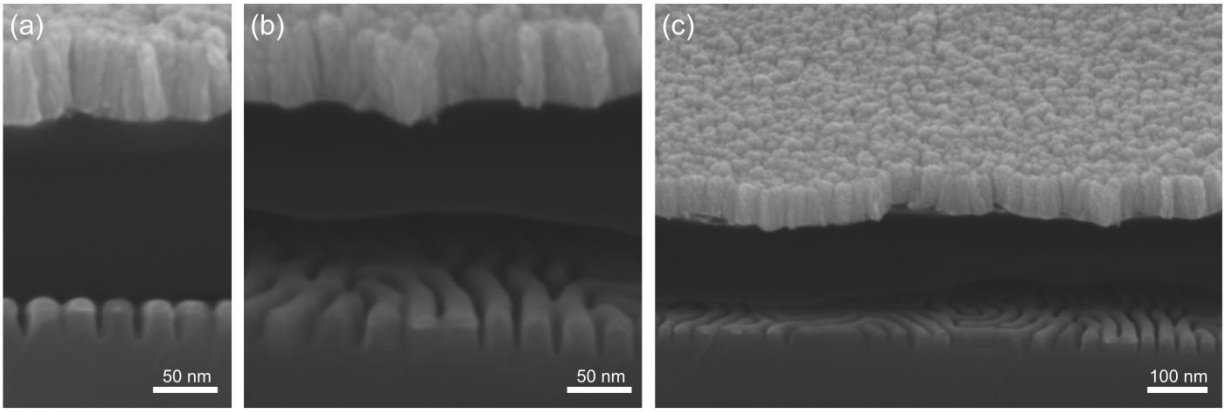

Figure G: SE image of Sample type 3 coated with PMMA (Mw=495k) and Au/Pd at **(a)** M=200k and 0 degrees tilt, **(b)** M=200k, 20 degrees tilt and **(c)** M=100k, 20 degrees tilt.

PMMA (**Figure G**) was found to exhibit very strong beam damage, causing the polymer to shrink by 75% and a tendency to pull back upon irradiation.

PMMA gives high contrast to imaged features and exhibits better trench filling properties without voids than the used conductive polymer. This was expected, as it is also a common resist material in e-beam lithography. PMMA coating gave good high contrast results, most likely due to the strong electron beam absorption, causing bond breaking of the polymer chains. PMMA thickness for imaging however is difficult to control, as the beam damage shrinks the polymer by up to 75% during imaging.
PMMA is non-conductive, in comparison to Aquasave. Therefore, if charging was a main contributor to the image quality, visibility of features should strongly degrade. Small features however can be imaged as well by using non-conductive PMMA. Therefore charging does is not seen to strongly affect the image.
Instead, we see a lower gray level background, compared to Aquasave. This shows, that apart from the scattered electron blocking mechanism in a stacked coating, the type of polymer also affects the contrast. As atomic densities (Z) of polymers are very similar, BSE interactions will be similar as well. It is known that the SE yield of polymers is more complex to measure than that of metals[11]. However, PMMA bonds are known to break in e-beam exposure[12] and thus SE are much better absorbed. This strong interaction of PMMA does explain the strong beam damage. Eventually, this also causes a lower yield and thus darker appearance.

Sup. H Coating variations – Carbon

Sample type 3: Patterned SiO_2 with Cr mask (30 nm pitch). Fabrication was done like Sample 2, but Cr mask was left on and pattern is not etched as deep as Type 2.

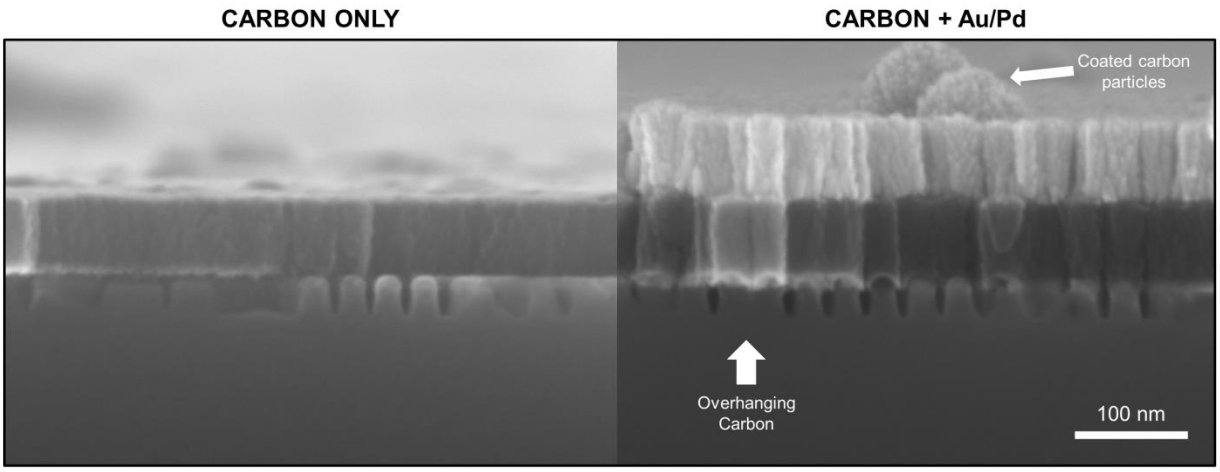

Figure H (left) SE image of Evaporated carbon on sample type 3. Note the overhang on the left, and right, while a small of the features in the center is well visible. Carbon does not break well. **(right**) Sample type 3 coated with carbon and Au/Pd. Carbon overhangs also visible, as well as particles from the carbon evaporation. The contrast mechanism, is also visible in this configuration, where low density carbon is covered by a high density Au/Pd.

Carbon (**Figure H**) has been found to promote contrast enhancement as well, but is difficult to work with. Carbon produces dust and particles tend to fall down on the sample. Also the thickness cannot be tuned as well in pointed rod evaporation compared to Au/Pd sputtering. Carbon has been found to also not break well, compared to the Aquasave or PMMA. Positive however is, that carbon evaporation is eventually cheaper than Aquasave, depending on the sample size to be coated and reusability of carbon rods or fiber.

Sup. I Residual free removal of CPM coating

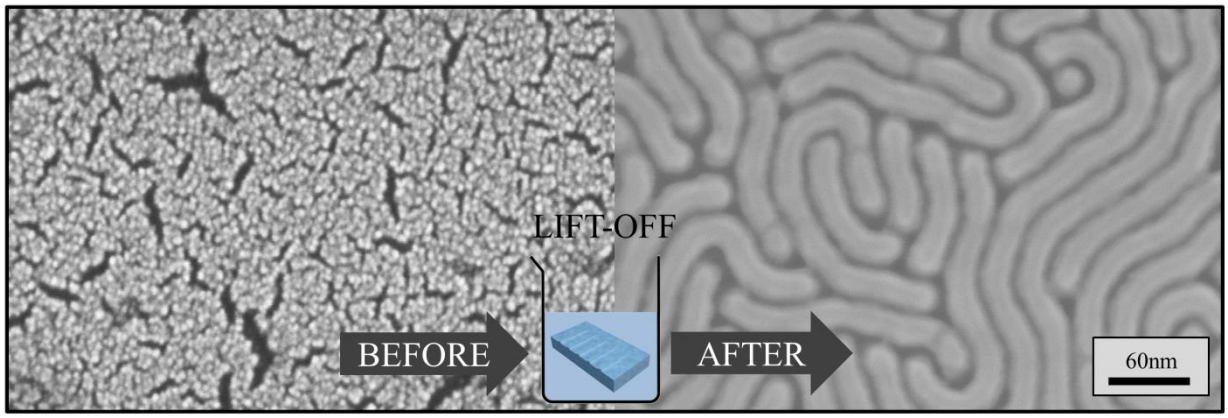

Figure I: SE image of top down SEM image of sample type 3 with CPM coating. **(left)** Before lift-off; **(right)** After a few seconds in water the metal layer lifts-off and exposes the fingerprint SiO_2 pattern.

Literature

1 S. Bhadra and D. Khastgir, *Polym. Degrad. Stab.*, 2007, **92**, 1824–1832.

2 S. Bhadra, D. Khastgir, N. K. Singha and J. H. Lee, *Prog. Polym. Sci.*, 2009, **34**, 783–810.

3 M. Pedersen, A. Rlzzi, J. Y. Hardeberg and G. Slmone, in *Society for Imaging Science and Technology - 4th European Conference on Colour in Graphics, Imaging, and Vision and 10th International Symposium on Multispectral Colour Science, CGIV 2008/MCS'08*, 2008, pp. 253–258.

4 D. G. Pelli and B. Farell, *J. Opt. Soc. Am. a-Optics Image Sci. Vis.*, 1999, **16**, 647–653.

5 D. G. Pelli and P. Bex, *Vision Res.*, 2013, **90**, 10–14.

6 A. Rose, *J. Opt. Soc. Am.*, 1948, **38**, 196–208.

7 J. Goldstein, D. Newbury, D. Joy, C. Lyman, P. Echlin, E. Lifshin, L. Sawyer and J. Michael, *Scanning Electron Microscopy and X-Ray Microanalysis*, Springer Science+Business Media, New York, 3rd edn., 2007.

8 H. Demers, N. Poirier-Demers, A. Réal Couture, D. Joly, M. Guilmain, N. de Jonge and D. Drouin, *Scanning*, 2012, **33**, 135–146.

9 M. Kotera, R. Ijichi, T. Fujiwara, H. Suga and D. B. Wittry, *Jpn. J. Appl. Phys.*, 1990, **29**, 2277–2282.

10 C. Gaillard, P. a Stadelmann, C. J. G. Plummer and G. Fuchs, *Scanning*, 2004, **26**, 122–130.

11 R. F. Willis and D. K. Skinner, *Solid State Commun.*, 1973, **13**, 685–688.

12 H. Duan, J. Zhao, Y. Zhang, E. Xie and L. Han, *Nanotechnology*, 2009, **20**, 135306.